Article

Coupled System of Dual-Axis Clinostat and Helmholtz Cage for Simulated Microgravity Experiments

Maciej Malczyk [1], Tomasz Blachowicz [1,*] and Andrea Ehrmann [2]

1   Institute of Physics—Center for Science and Education, Silesian University of Technology,
     44-100 Gliwice, Poland; mmalczyk@polsl.pl
2   Institute for Technical Energy Systems (ITES), Faculty of Engineering and Mathematics, Bielefeld University
     of Applied Sciences and Arts, 33619 Bielefeld, Germany; andrea.ehrmann@hsbi.de
*   Correspondence: tblachowicz@polsl.pl

Abstract: The experimental investigation of plant growth under space conditions is a necessary prerequisite of long-term space missions. Besides experiments in space, many studies are performed under simulated microgravity, using a clinostat. However, the Earth magnetic field is usually not taken into account in such investigations. Here, a self-designed and constructed system of coupled devices—a clinostat and a Helmholtz cage—is presented. The clinostat can, on average, cancel the effective gravity field by using two independent rotations, enabling simulated zero-valued gravity experiments. Additionally, an appropriately symmetrically mounted Helmholtz cage can be used to cancel the natural Earth magnetic field in the volume where the clinostat is located. The combination of these two devices offers the opportunity, e.g., for bio-inspired experiments in which plant cultivation can be carried out in conditions that imitate a space environment. We provide information about the experimental setup and show first experimental results of growth tests.

Keywords: clinostat; Earth magnetic field; simulated microgravity; plant growth

1. Introduction

Plant cultivation in special physical circumstances, especially in different magnetic and gravitational conditions, is a relatively new research trend related to the development of space technologies. It is necessary, however, since plants are known to be influenced by gravitropism, resulting in roots growing downwards while shoots grow upwards, led not only by light, but also by gravity [1–3].

Such research can be carried out in two different ways. The first one relies on sending samples into space [4] and placing them on board the International Space Station (ISS) [5–7]. This approach is relatively expensive and limited by the capabilities of today's space technology. The second method is to arrange experiments in conditions similar to those met in space. A common approach to simulate plant growth in space is given by a clinostat, which constantly changes the plant orientation, so that, on average, all directions are indistinguishable [8,9]. Typically, rotational speeds of around 1 rpm are used for plant experiments [10], while rotations that are too slow may lead to helical plant growth [11].

Comparisons of experiments in a clinostat and in real microgravity often show similar results, as long as suitable rotational speeds are chosen [12,13]. Nevertheless, another important impact on plant growth, besides gravity, is often disregarded: the Earth magnetic field with its induction of the order of 45 μT = 0.045 mT. Magnetic fields with a broad range of magnitudes have been investigated with respect to their impact on plant growth. Static and alternating magnetic fields of 400 mT and 30 mT, respectively, were shown to positively impact the seed germination and chlorophyll content of soybean seeds, respectively [14]. Static magnetic fields between 420 mT and 580 mT were also found to increase the root growth of *Arabidopsis thaliana* [15]. By applying a static magnetic field of 110 mT, the growth of *Pelargonium graveolens* could be improved regarding plant height, root length,

chlorophyll content, and other parameters [16]. While such relatively large magnetic fields are mostly regarded as positive for plants, only a few experiments were found on the influence of switching off the Earth magnetic field, and those showed often inconsistent or irreproducible results [17–20], underlining the importance of further investigating plant growth in a zero magnetic field for future space missions as well as the influence of μT fields on the biological species important for a living environment. Shielding the Earth magnetic field is possible with a Helmholtz cage [21], as is described in the next section. It should be mentioned that descriptions of a clinostat inside the homogeneous magnetic field of a Helmholtz cage are only scarcely found in the literature. Yamashita et al. report a pair of Helmholtz coils at the ends of the moving stage of a clinostat, i.e., the possibility to influence the inner part of the clinostat chamber by a magnetic field, which is moved together with the sample chamber and thus not able to counteract the Earth magnetic field or to apply a magnetic field along a defined orientation with respect to the laboratory inertial system [22]. Mo et al. mentioned the importance of taking the hypomagnetic field far away from Earth into account in future simulations of biological responses for outer space missions, but while explicitly suggesting shielding the Earth magnetic field in clinostat experiments, no corresponding instrument was reported [23]. Only one paper was found that described cancelling the Earth magnetic field as well as using a clinostat for simulated microgravity [24]; however, the tested biological samples were only exposed to one of these specific conditions.

Usually, previous experimental studies concentrated on investigating the influence of either the modified magnetic field [25–27] or simulated microgravity only [28–31].

Here, we report the construction, electrical configuration and software for a system consisting of a two-axial two-frame clinostat and a Helmholtz cage large enough to be coupled with the clinostat. We also show preliminary bio-inspired results of experiments in a clinostat with beans as an example of simple edible plants. Our proposal, with its mechanical, electronics, sensing and software content, is original and does not contain any copies of existing solutions, though it is based on available materials and components.

2. Design and Construction

2.1. Principle of Clinostat Operation

The two-axis clinostat developed in a recent project, also called a random positioning machine [32], consists of an aluminum frame (Figure 1) that rotates relative to the clinostat base that is also made of aluminum. Inside the rotating frame, a spherical region rotates independently, where experiments in simulated microgravity can be carried out. In the sphere, several physical parameters, such as acceleration, angular velocity, temperature, humidity, and light intensity, can be measured and sent remotely to an external computer. Moreover, the cultivation area can be observed by a camera, providing online visual information about the growth progress.

The two rotations—one of the frame and one of the cultivation sphere—create a situation in which the average effective value of gravity is reduced to zero. Because of this, plants are not able to sense gravity's direction and are thus forced to grow in a state similar to weightlessness in cosmic space. The ratio of angular velocities—of the frame and the sphere—define the number of turnovers for which the optimum conditions of average zero-gravity will be achieved. Our calculations and tests showed that the ratio of 1:2.2 (frame to sphere velocities) also gave the lowest mean gravity fluctuations, leading to values between 0.0657 g and 0.0072 g. Since the axes operate at constant speeds, the devices belong to a 3D clinostat class. Figure 2 depicts the results of time-dependent measurements of the acceleration components using built-in accelerometers. Additionally, which is worth noting, the angular velocities have to be kept at low values to obtain satisfactory conditions for plant growth, especially if taking into account the spatial distribution of humidity in the cultivation area [33]. Thus, we usually used a velocity of 0.31 rad/s for the frame and 0.68 rad/s for the sphere.
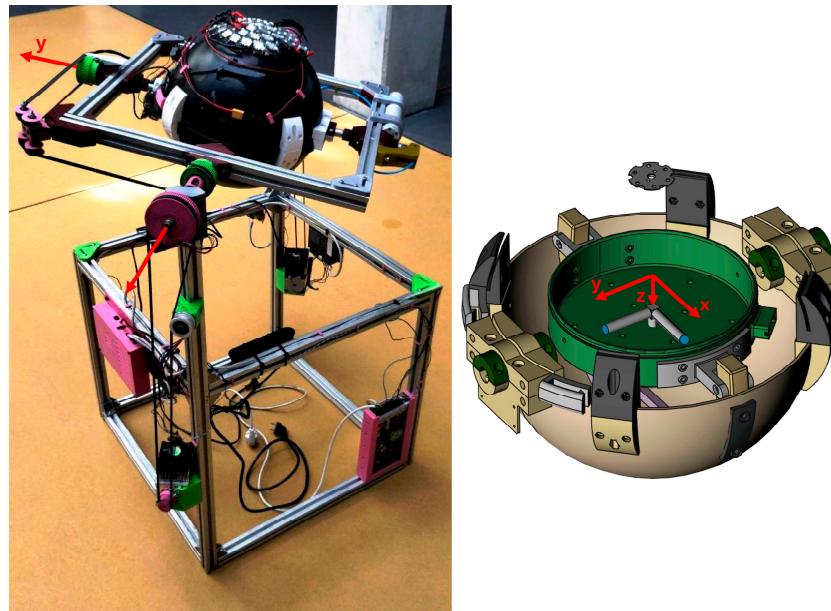
Figure 1. Designed and constructed clinostat (left panel) with the centrally mounted, optically isolated, spherical area (diameter of 300 mm) in which the micro-gravity experiment can be carried out. The system is powered by two stepper motors (one visible in front at the vertical edge and the second symmetrically mounted at the vertical edge in the back) and a system of rubber stripes along with transmission gears. The axes of rotations are marked by red arrows. In the bottom-right corner, the control unit for the stepper motors is visible. The box on the left, mounted at the upper horizontal edge, is the main control computer. On top of the sphere, the system of LEDs (light emitting diodes) illuminating the cultivation process is visible. The right panel presents the spatial orientation of the three-axis magnetic-field sensor (LIS3DH, Adafruit® (Brooklyn, NY, USA)) located in the cultivation sphere.
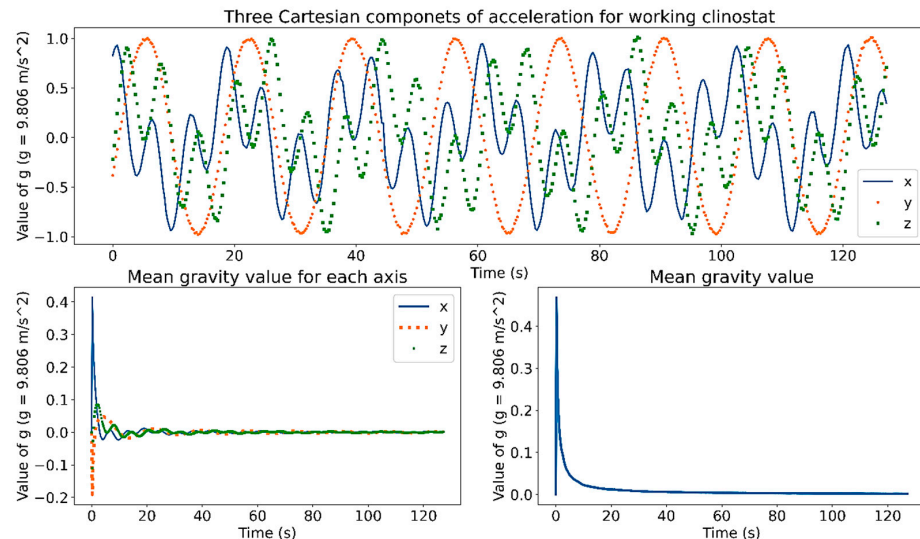

Figure 2. Results of measured gravitational acceleration components (x, y, z) in the rotating clinostat with an angular velocities ratio (frame to sphere) equal to 1:2.2. In the top panel, the temporary values are given. In the bottom-left panel, the averaged values of gravitational acceleration components (x, y, z) are provided, while in the bottom-right panel, the absolute (square root of the squares of three acceleration-component instantaneous values), the averaged value of g is presented. To measure the gravity, the three-axis LIS3DH (Adafruit®) acceleration sensor was used and mounted in the center of the cultivation sphere (comp. Figure 1). The normal, static g acceleration is parallel to the vertical direction in the laboratory room.

2.2. Mechanical Components of the Clinostat

In the construction process, we strictly applied the postulate to limit ferromagnetic material as much as possible. Timing gears, pulleys, construction connectors for the clinostat frames, and the other cultivation parts are made of poly (lactic acid) (PLA) or polyethylene terephthalate glycol (PETG) filaments using 3D-printing technology. The cultivation sphere is made from polyester, and its parts are connected with screws and bolts made of nylon.

The mechanical part of the clinostat consists of the static mechanical housing and the cultivation area. The frames are made of typical V-SLOT-type aluminum profiles. The metal parts were cut and formed with the use of a milling machine, and the assumed accuracy is below 0.1 mm. The "plastic" parts were printed using a 3D printer with 0.2 mm accuracy. The angular uncertainty of perpendicularly mounted parts is below one angular degree. We do not test what might be the maximum deformation for a heavy load. In recent experiments, we used a payload with a mass of about 1 kg and did not notice any significant deformation effects in the whole construction. The cultivation chamber was adopted from a commercially available geographical globe. The rotating alumina frame is driven by two-timing gears and one belt (cf. Figure 1—the motor mounted at the back vertical edge). To pass rotation from the second stepper motor to the sphere, a two-timing belt mechanism was used. The rotating frame axle is mechanically independent from the sphere axle, whereby it can rotate at its own speed and can change orientation. The gearbox is kinked at a right angle and the belt is guided with idler pulleys to power sphere rotations. Each timing belt has its independent tensioning mechanism. The axles are made of aluminum pipes in which water pipes and electrical cables are embedded. The water supply system is made of a peristaltic pump (DP-DIY type, 12 VDC, efficiency of 5–10 mL/min, made by INTLLAB® (Seri Kembangan, Malaysia)), polyurethane tubes of internal diameter equal to 2 mm, rotational connectors, and perforated silicon tubes located close to the cultivation area. A peristaltic pump prevents reversing water flow. To reduce angular velocity fluctuations resulting from uneven weight distribution, additional counterweights were used—for example, to balance the LED lighting system.

The cultivation process has to be protected from external light sources to keep it controlled. The sphere has a diameter of 320 mm (Figure 3) and is divided into two semi-spheres to allow access and enable the preparation of seeds, cleaning, and harvesting. Inside the sphere, there is a plastic cylindrical basket with a radius of 95 mm, located symmetrically at the main cross-section, which is the base for cultivation. Directly attached to the plastic sphere, a second (apart from the main computer mounted to the main frame—cf. Figure 1) small, single-board computer of the Raspberry Pi type is used to acquire data from sensors. The clinostat stepper motors (Nema 24 manufactured by Nanotec®) have 4 Nm torque. Each motor is driven by a DM556 stepper motor driver manufactured by Leadshine®. The total size of the clinostat fits a volume of 620 mm width and length, respectively, and a 963 mm height.

In addition to the clinostat, a static copy—the reference device—was constructed. It is used to compare results from the zero-mean-gravity experiment to normal-Earth-gravity circumstances. Figure 4 shows the static version.

2.3. Electrics and Sensors of the Clinostat

Electric power is provided to the microcomputer and LEDs with cables that are run inside aluminum profiles and axles. Due to rotations of the construction elements, special slip rings with up to 12 connectors were used (KYM12B type made by Asiantool® (New Taipei, Taiwan)).

In the cultivation area, diverse sensors are applied to monitor the experiment. Two temperature sensors (MCP9808 (Adafruit®)) at opposite positions measure the temperature. Light-intensity sensors (APDS9960 (Adafruit®)) are placed on basket guides. The soil moisture sensor is made of two aluminum rods mounted parallelly and distanced with plastic spacers. The three-axis LIS3DH (Adafruit®) acceleration sensor is mounted in the

center of the sphere to monitor the microgravity state. Additionally, two cameras are added to take pictures of cultivated plants.
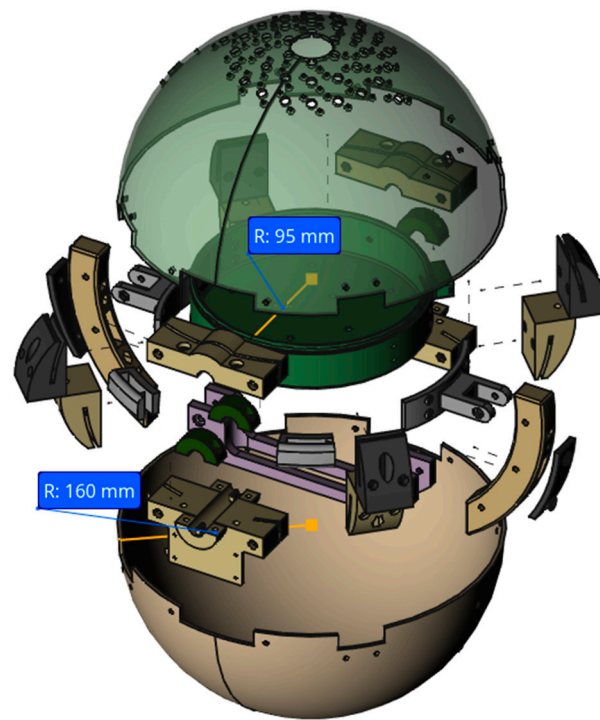

Figure 3. A 3D view of the cultivation sphere and the construction details.
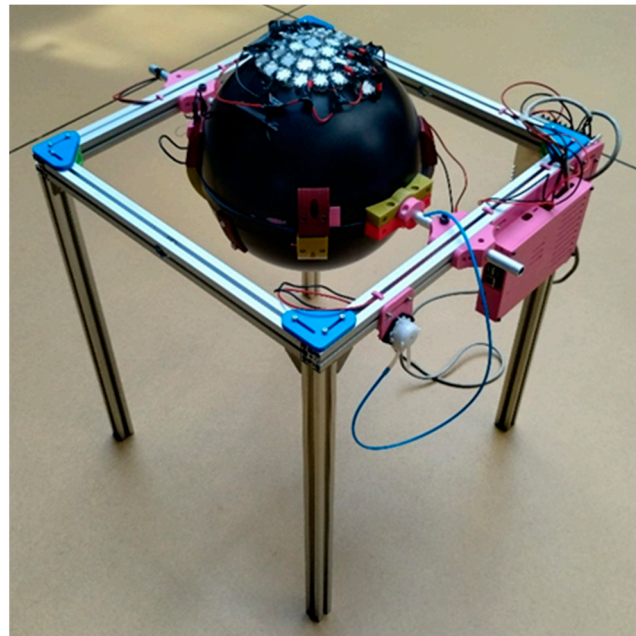

Figure 4. The static version of clinostat offers the opportunity for natural Earth gravity experiments and comparative studies.

The LED illuminator, shown in Figure 5a, consists of 24 red (PK2N-3LME-HSD, 650–670 nm, 3 W), 10 blue (PM2E-3LBS-SD, 455–475 nm, 3 W), and 5 white diodes (PM2E-3LVS-R7, 3 W), manufactured by ProLight Opto® (Taoyuan City, Taiwan). Each one has a maximum power of 3 W. The total mass of diodes with radiators equals 273 g. The number of diodes and colors was chosen in such a way to mimic the spectrum supporting

the photosynthesis of plants [34]. Light intensity is controlled with a 12 V pulse width modulation (PWM) signal. Each diode has its radiator to remove heat. Diodes are mounted on the upper half of the sphere and point toward the basket. The position of diodes was examined by Monte Carlo simulations to find the uniform illumination area (Figure 5b).
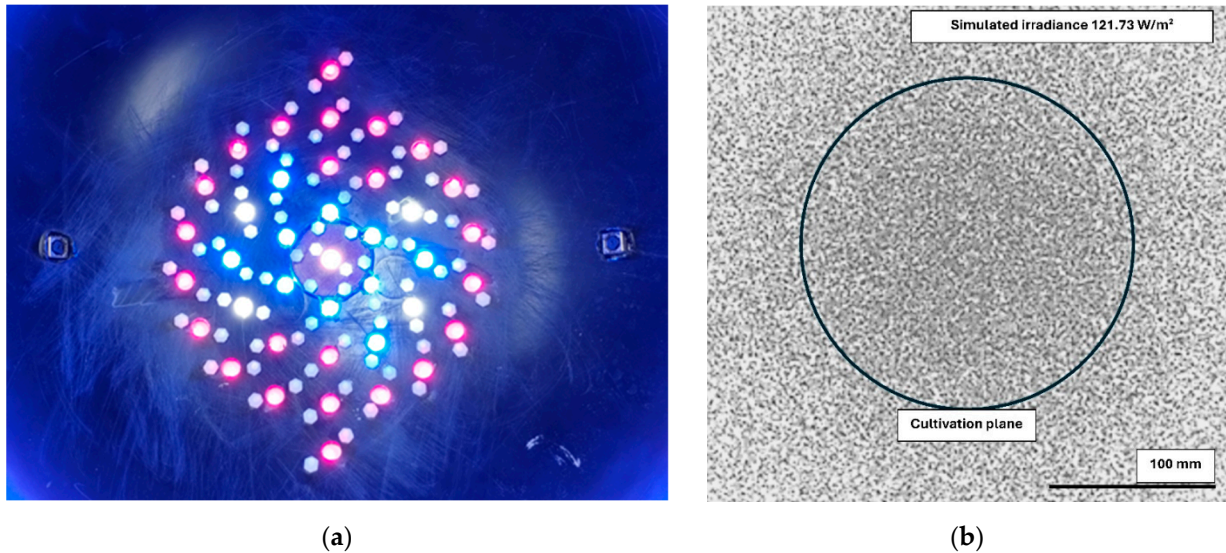

(**a**)   (**b**)

Figure 5. The LEDs mounted in the upper semi-sphere (**a**) and the simulated light-intensity spatial distribution at the cultivation plane showing uniform illumination (**b**).

The main clinostat computer (Raspberry RPi4) controls the motors, light intensity of diodes, and water pump flow. The second computer (Raspberry Pi Zero W) was mounted on the sphere to collect signals from sensors and cameras. The general view of clinostat signal flow is given in Figure 6. Details about computer (cultivation, controller) signals are seen in Figure 7. Details about the relay block and the opto-isolation block are explained in Figures 8 and 9, respectively. The control of a pump by the RPi4 computer met some electric incompatibility. The current that can be taken from the RPi4 IO pins is too low for powering devices, so a solution with a BC547 transistor was applied to pass enough amount of energy. Similarly, the lighting control circuit uses the IRF540N MOSFET to control the LED's lighting system.
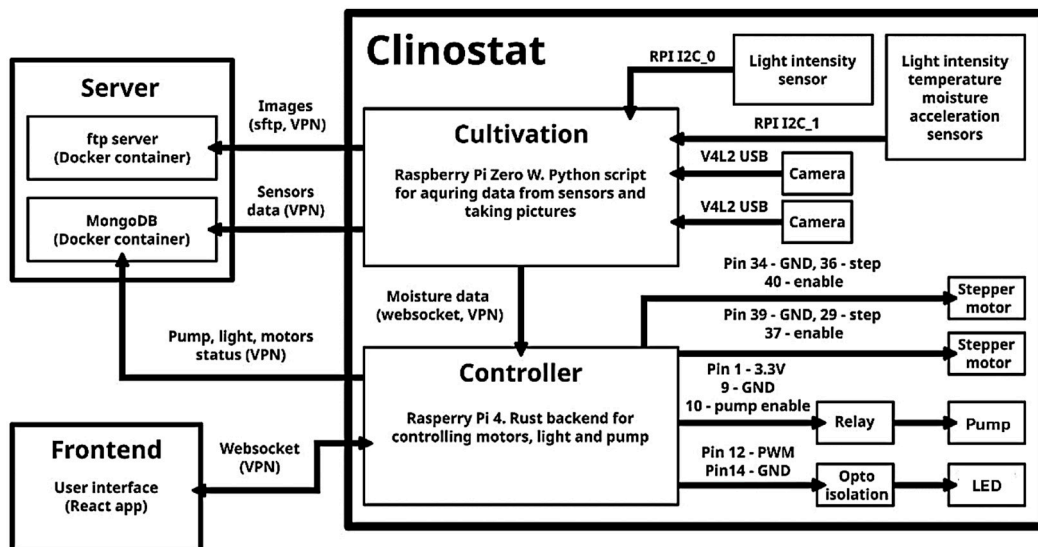

Figure 6. Blocks diagram of the signal flow for the clinostat system. The server is an external desktop computer.
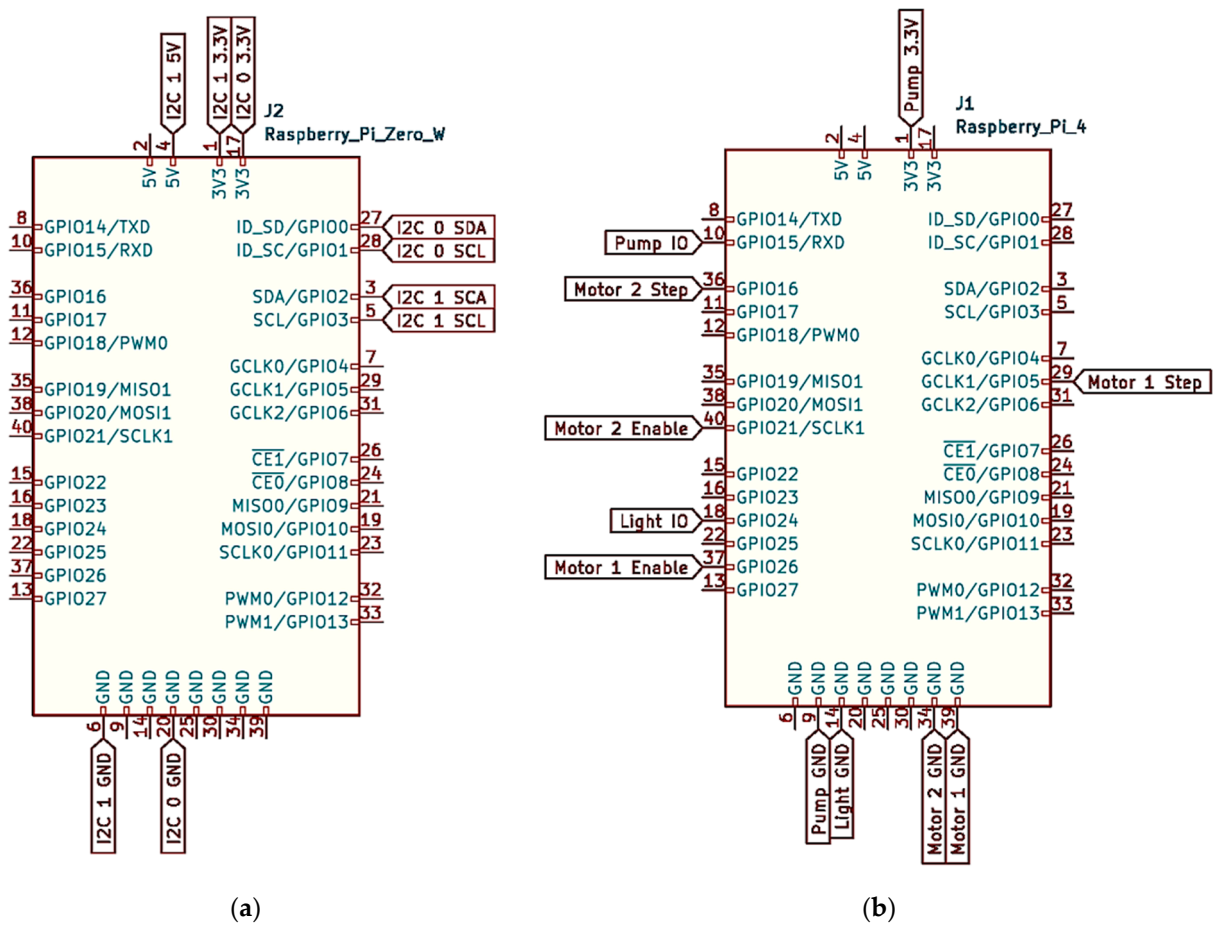
Figure 7. Electric diagram of connections and control signals (**a**) for the cultivation sphere computer, Raspberry Pi Zero W, and (**b**) for the main clinostat computer, Raspberry RPi4 (on the right).
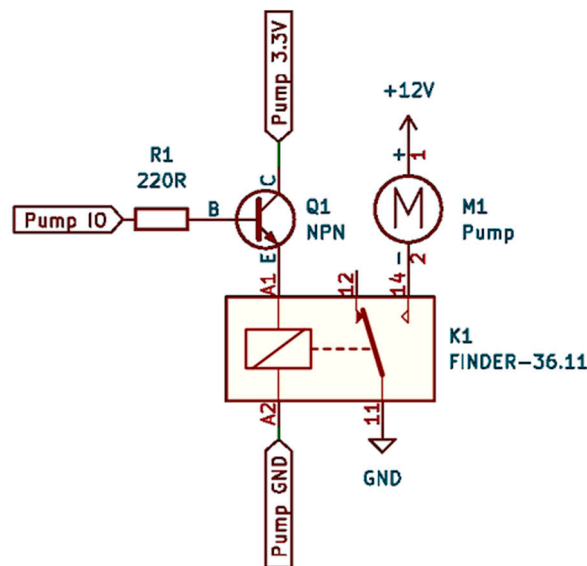

Figure 8. Details of current supply of the pump where transistor base (Q1, BC547) is controlled by the pump IO signal, and where the electric relay K1 is applied.
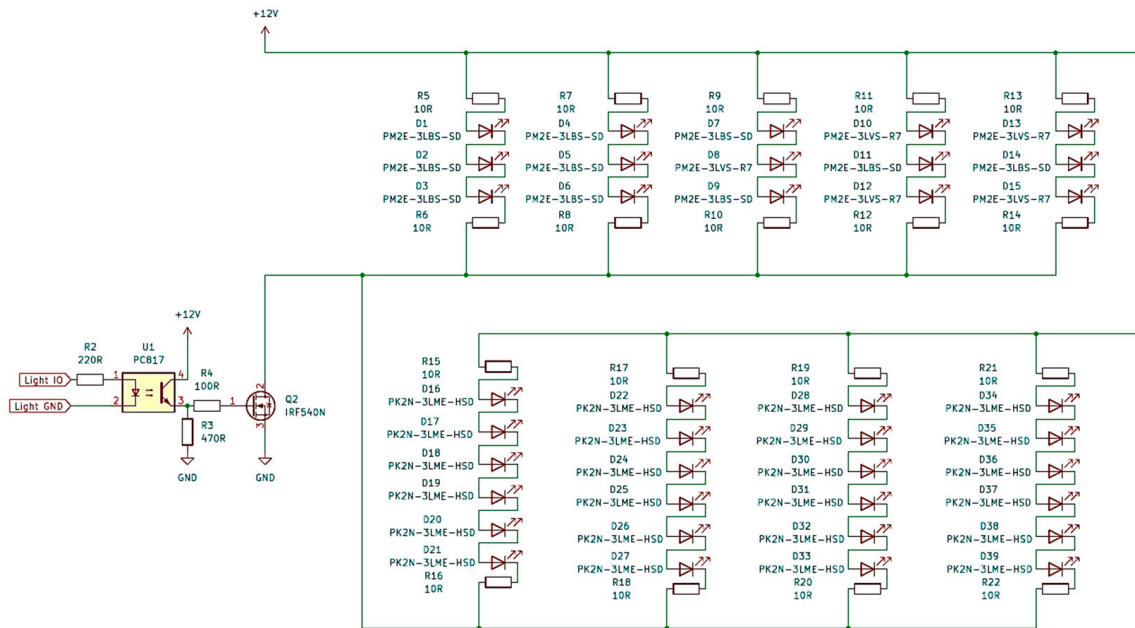
Figure 9. Electric diagram of LEDs' control and electric supply of the lighting system. The opto-transistor PC817 controls the MOSFET IRF540N gate.

2.4. Clinostat Software

A part of the software associated with the image processing of the cultivation area is written in Python on the basis of a so-called microservice conception, which is commonly used in network applications. Each component is treated as an elementary networked service that can be connected to a hardware device or to another software part. Each service sends data or responds to requests from other services. The WebSocket protocol is used in this way to communicate between all the parts (cf. Figure 6).

Image acquisition is realized by Python script that utilizes the sftp protocol, while the captured images are processed with the Open CV library. They are saved to the file system and sent remotely to the external sftp server to release local memory. Hence, the file names are sent to the external MongoDB [35] database as HTTP strings, so everyone connected via the VPN service to the system computer can open each image in a browser.

The main clinostat software controls the motors, light, and pumps. It is written in Rust Programming Language [36] using the so-called Tokio library [37]. Tokio is an asynchronous input/output framework for Rust, and it is used for network communication between parts with the use of WebSockets protocols.

The user interfaces for the clinostat and the cage were realized using the React framework [38] and the Electron framework [39], respectively. The choice of such tools was arbitrary, and the only reason was to test these and become familiarized with them. The frameworks utilize component ideology; each element of the web page can be symbolized as a programmable block, which has its functionalities and can share its properties. The component can be independently refreshed, so if new data come from the system, information will be updated at the frontend, i.e., the user interface layer. The clinostat frontend enables the control of light intensity, moisture, and angular velocities, while the cage frontend controls electric parameters.

2.5. The Helmholtz Cage

The constructed Helmholtz cage is a device that can modify the magnetic field inside its central part, where the clinostat can be located. The cage is built from three pairs of octagonal coils, with the biggest one inscribed in a circle of diameter 2 m; the other two pairs of coils are slightly smaller, to be mounted inside the largest coils. 90 turns per coil were wound on alumina skeletons using 1.2 mm diameter copper wire. The octagonal

coil shape was chosen because of its induction properties being very close to those of a circle, while the mechanical construction is simple enough. It is worth mentioning that in the simplest case, square cages are commonly used [40–42], but they have limited magnetic-field homogeneity.

The cage is powered with three Rigol® (Suzhou, China) DP811 variable power supplies (Figure 10). Each supply powers one Helmholtz coil pair. The maximum power that can be delivered to one pair of coils equals 100 W (20 V, 5 A).
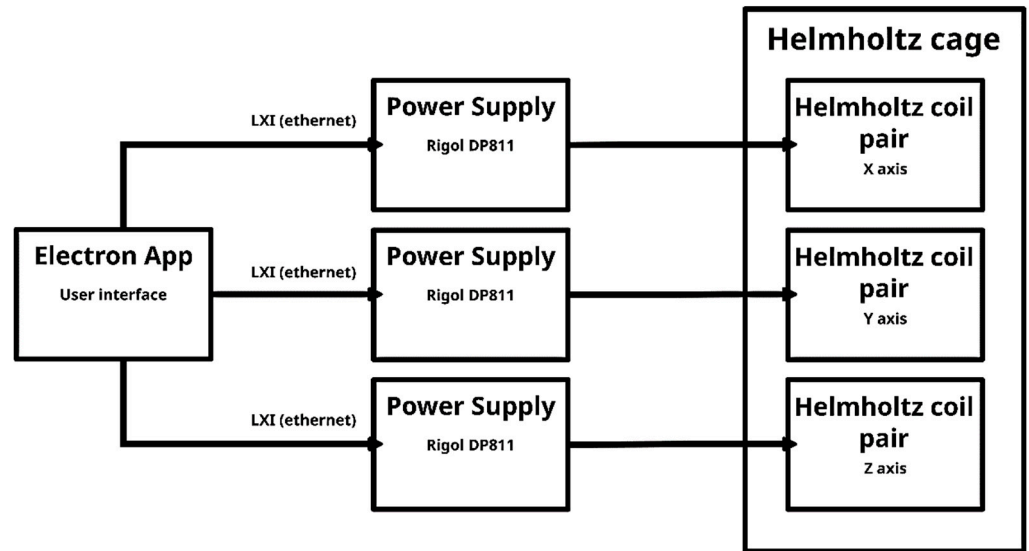
Figure 10. Block diagram of the control signal flow for the Helmholtz cage.

To find the magnetic-field spatial distribution inside the cage, adequate calculations, on the base of Ampere's law using a custom-made Python code, were performed. The imposed condition of about 1% deviation from the field value in the cage center (located 1 m above the construction base) resulted in the determination of the optimum experimental region of homogeneity. In Figures 11 and 12, the results of simulations are presented for different numbers N of hypothetical coil polygon sides (we used N = 8). The simulation was further validated with measurements inside the built Helmholtz cage.
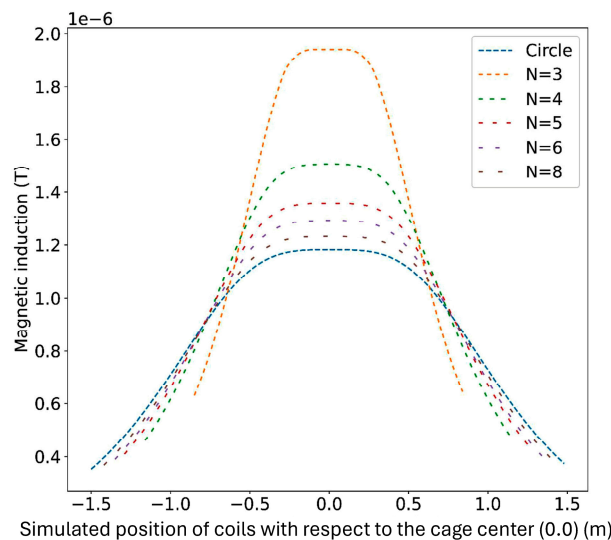

Figure 11. Results of simulation of magnetic-induction spatial distribution at the vertical main cross-section of the Helmholtz cage. In the real construction, the N = 8 case was chosen and the distances from the center of Helmholtz cage were equal to +/−492 mm, +/−471 mm, +/−440 mm.
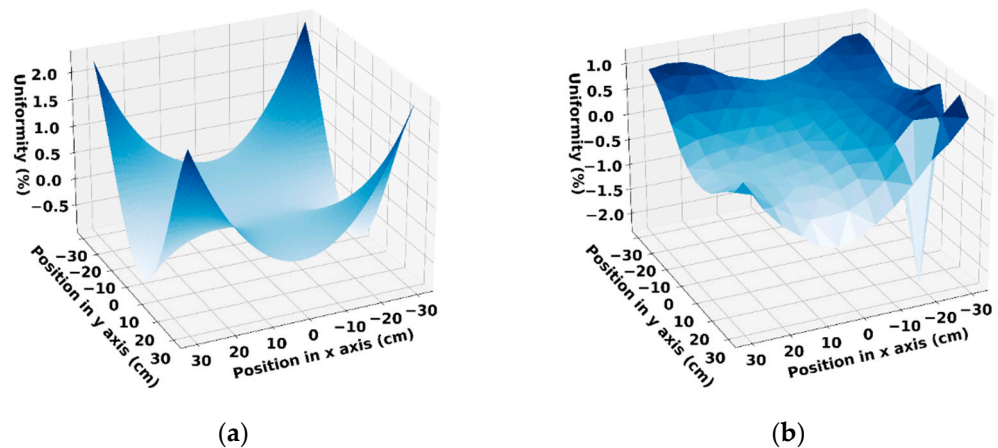
Figure 12. (**a**) Results of simulations and (**b**) the measured magnetic-field values inside the central region of the Helmholtz cage. The measurements were carried out with the AlphaLab Milligauss MR3 magnetometer.

As mentioned earlier, the clinostat and the Helmholtz cage were designed to be complementary, in the sense that they are dimensionally compatible (Figure 13)—the center point of the cultivation sphere is identical to the middle of the cage. Importantly, the diameter of the sphere is comparable with the previously simulated region (0.4 m × 0.4 m × 0.4 m), possessing adequate field homogeneity.
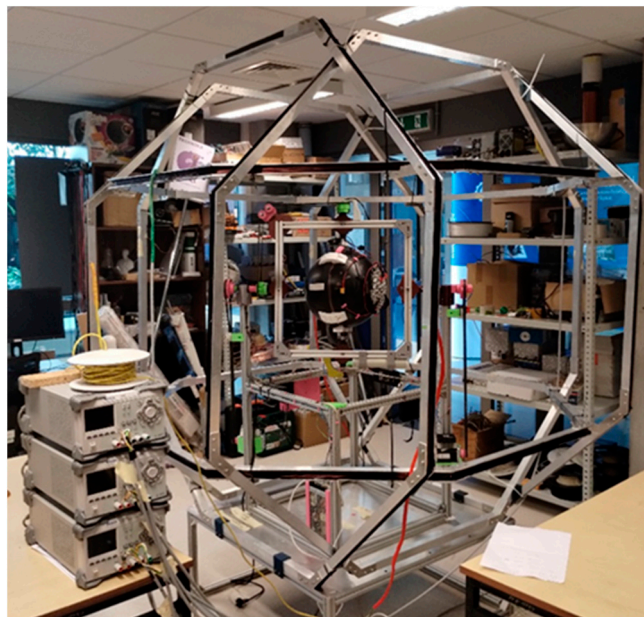

Figure 13. The general view of the experimental system. Inside the Helmholtz cage, the clinostat is placed.

We did not assume rapid changes of Earth magnetic field during experiments. Using simulations and direct measurements, at the initial phase of the experiment, we are able to find such conditions in which the Earth magnetic field is compensated. In the laboratory, we did not notice any long-term fluctuations of the field. Looking at Figure 12, the magnetic field's spatial uniformity in the central region of the cage is better than 2%. For a typical value of the magnetic-field induction equal to about 45 µT, the 2% time fluctuations of the field are equivalent to about 0.9 µT. It can be assumed that the presented setup will work with such accuracy in the static-field mode. However, for future long-time experiments, the system should be updated to closed-loop active-field compensation.

2.6. Cultivation Experiments

To investigate the clinostat's effect on plant growth, we performed several preliminary cultivations (Figures 14 and 15). We used *Lepidium sativum* L. (Figure 14) and *Phaseolus coccineus* L. (Figure 15) as test plants because they are easy to grow and have a short vegetation period. The figures present the two one-week growth results in the clinostat and in the reference static sphere. Videos of the cultivation process of *Phaseolus coccineus* L. can be obtained on request from authors. Gravitropism is highly visible in all the plant's parts: stems, roots, and leaves. Cotton was used as a substrate material because of its good water-retention capabilities. In the first experiments to block the movement of the breeding, a properly perforated foil with holes was used. This is not the only solution. It is also possible to use the appropriate mesh made of plastic material. The results have preliminary characteristics, and future experiments in a variety of circumstances will be conducted, especially with the inclusion of magnetic-field variation.

Figure 14. Results of *Lepidium sativum* L. cultivations: (**a**) cultivation in the clinostat with humidity 35% and light 10% of its maximum value, (**b**) cultivation in the clinostat with humidity 75% and light 8% of its maximum value; the static cultivation results (**c**) and (**d**) corresponding to the conditions of (**a**) and (**b**), respectively.
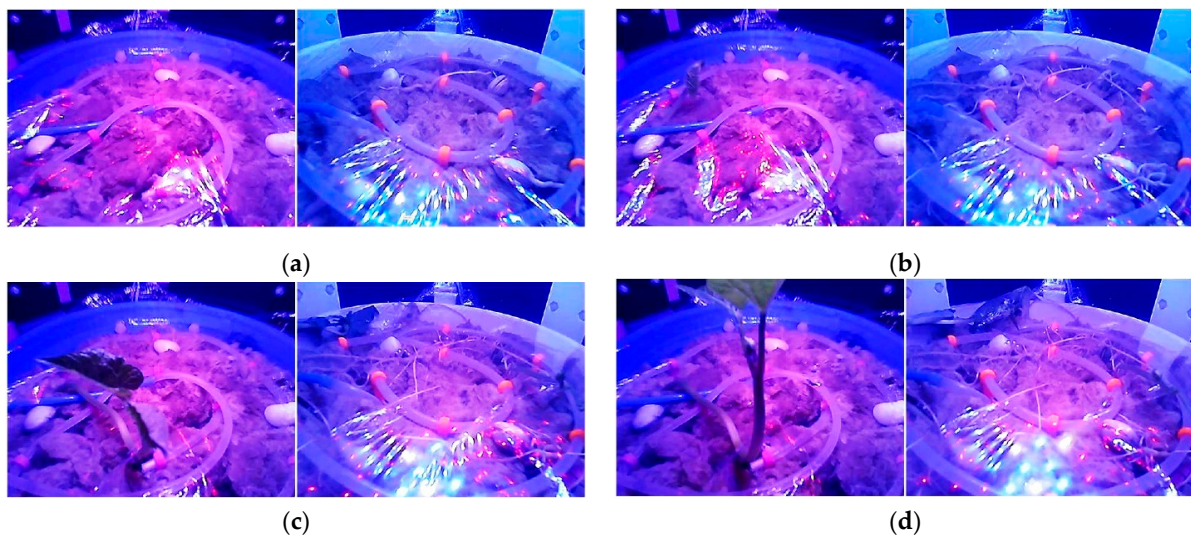

(**a**)

(**b**)

(**c**)

(**d**)

Figure 15. Results of *Phaseolus coccineus* L. cultivations. Each left panel shows results for normal gravity, while a right panel shows the simulated microgravity conditions. The photographs depict levels of growth after (**a**) 6 days, (**b**) 10 days, (**c**) 13 days, and (**d**) 14 days. In zero-gravity conditions, the plant cannot develop a root system around the dominant direction. Its growth is retarded, and the emerging leaf growth is chaotic.

3. Conclusions

In this manuscript, a clinostat with a surrounding Helmholtz cage was presented. The system enables plant growth under simulated microgravity with the Earth magnetic field cancelled out or modified, respectively. Due to the impact of both factors on plant growth, simulations of plant cultivation in space can be performed very conveniently, without organizing special orbital missions. The first experiments with *Lepidium sativum* and *Phaseolus coccineus* showed a significant difference between plants grown in simulated microgravity, i.e., in the clinostat, and under static conditions, i.e., in the usual Earth gravitational field. Future experiments will also be conducted in the presence of a magnetic field to show its impact on the dynamics of the growth of biological structures. Further research will also be conducted with microscopic objects, such as, for example, bacterial colonies. The authors hope that the information presented will also be useful for scientists who want to build their own similar experimental system.

References

1. Chen, R.J.; Rosen, E.; Masson, P.H. Gravitropism in higher plants. *Plant Physiol.* **1999**, *120*, 343–350. [CrossRef]
2. Mancuso, S.; Shabala, S. *Rhythm in Plants: Phenomenology, Mechanisms, and Adaptive Significance*; Springer: Berlin/Heidelberg, Germany; New York, NY, USA, 2007.
3. Blachowicz, T.; Ehrmann, A.; Malczyk, M.; Stasiak, A.; Osadnik, R.; Paluch, R.; Koruszowic, M.; Pawlyta, J.; Lis, K.; Lehrich, K. Plant growth in microgravity and defined magnetic field. In Proceedings of the International Conference on Electrical, Computer, Communications and Mechatronics Engineering (ICECCME), Belle Mare, Mauritius, 7–8 October 2021.
4. Driss-Ecole, D.; Legué, V.; Carnero-Diaz, E.; Perbal, G. Gravisensitivity and automorphogenesis of lentil seedling roots grown on board the International Space Station. *Physiol. Plant.* **2008**, *134*, 191–201. [CrossRef]
5. Vegetable Production System (Veggie). Available online: https://ntrs.nasa.gov/api/citations/20160005059/downloads/2016000 5059.pdf (accessed on 29 June 2024).
6. Veggie. Available online: https://www.nasa.gov/wp-content/uploads/2019/04/veggie_fact_sheet_508.pdf (accessed on 29 June 2024).
7. Zabel, P.; Bamsey, M.; Schubert, D.; Tajmar, M. Review and analysis of over 40 years of space plan growth systems. *Life Sci. Space Res.* **2016**, *10*, 1–16. [CrossRef]
8. Hoson, T.; Kamisaka, S.; Buchen, B.; Sievers, A.; Yamashita, M.; Masuda, Y. Possible use of a 3-D clinostat to analyze plant growth processes under microgravity conditions. *Adv. Space Res.* **1996**, *17*, 47–53. [CrossRef]
9. Theoret, N. Attitude Determination Control Testing System (Helmholtz Cage and Air Bearing). Honors Thesis, 2783. Western Michigan University, Kalamazoo, MI, USA, 2016.
10. Boucheron-Dubuisson, E.; Manzano, A.I.; Le Disquet, I.; Matía, I.; Sáez-Vasquez, J.; van Loon, J.J.; Herranz, R.; Carnero-Diaz, E.; Medina, F.J. Functional alterations of root meristematic cells of Arabidopsis thaliana induced by a simulated microgravity environment. *J. Plant Physiol.* **2016**, *207*, 30–41. [CrossRef]

11. Sievers, A.; Hejnowicz, Z. How well does the clinostat mimic the effect of microgravity on plant cells and organs? *ASGSB Bull.* **1992**, *5*, 69–75.

12. Lorenzi, G.; Perbal, G. Root growth and statocyte polarity in lentil seedling roots grown in microgravity or on slowly rotating clinostat. *Physiol. Plant.* **1990**, *78*, 532–537. [CrossRef]

13. White, J. Formation of red wood in conifers. *Proc. R. Soc. Vic.* **1908**, *20*, 107–124.

14. Michalak, I.; Lewandowska, S.; Niemczyk, K.; Detyna, J.; Bujak, H.; Arik, P.; Bartniczak, A. Germination of soybean seeds exposed to the static/alternating magnetic field and algal extract. *Eng. Life Sci.* **2019**, *19*, 986–999. [CrossRef]

15. Jin, Y.; Guo, W.; Hu, X.; Liu, M.; Xu, X.; Hu, F.; Lan, Y.; Lv, C.; Fang, Y.; Liu, M.; et al. Static magnetic field regulates Arabidopsis root growth via auxin signaling. *Sci. Rep.* **2019**, *9*, 14384. [CrossRef]

16. Nyakane, N.E.; Sedibe, M.M.; Markus, E. Growth response of rose geranium (*Pelargonium graveolens* L.) to calcium:magnesium ratio, magnetic field, and mycorrhizae. *Hortscience* **2019**, *54*, 1762–1768. [CrossRef]

17. Dhiman, S.K.; Galland, P. Effects of weak static magnetic fields on the gene expression of seedlings of *Arabidopsis thaliana*. *J. Plant Physiol.* **2018**, *231*, 9–18. [CrossRef]

18. Harris, S.R.; Henbest, K.B.; Maeda, K.; Pannell, J.R.; Timmel, C.R.; Hore, P.J.; Okamoto, H. Effect of magnetic fields on cryptochrome-dependent responses in *Arabidopsis thaliana*. *J. R. Soc. Interface* **2009**, *6*, 1193–1205. [CrossRef]

19. Ahmad, M.; Galland, P.; Ritz, T.; Wiltschko, R.; Wiltschko, W. Magnetic intensity affects crypto-chrome-dependent responses in *Arabidopsis thaliana*. *Planta* **2007**, *225*, 615–624. [CrossRef]

20. Rakosy-Tocan, L.; Aurori, C.M.; Morariu, V.V. Influence of near null magnetic field on in vitro growth of potato and wild *Solanum* species. *Bioelectromagnetics* **2005**, *26*, 548–557. [CrossRef]

21. Magdaleno-Adame, S.; Olivares-Galvan, J.; Campero-Littlewood, E.; Escarela-Perez, R.; Blanco Brisset, E. Coil Systems to Generate Uniform Magnetic Field Volumes. In Proceedings of the Comsol Conference 2010, Boston, MA, USA, 7–9 October 2010.

22. Yamashita, M.; Tomita-Yokotani, K.; Hashimoto, H.; Taka, M.; Tsushima, M.; Nakamura, T. Experimental concept for examination of biological effects of magnetic field concealed by gravity. *Adv. Space Res.* **2004**, *34*, 1575–1578. [CrossRef]

23. Mo, W.C.; Liu, Y.; He, R.Q. Hypomagnetic field, an ignorable environmental factor in space? *Sci. China Life Sci.* **2014**, *57*, 726–728. [CrossRef]

24. Ogneva, I.V.; Usik, M.A.; Burtseva, M.V.; Biryukov, N.; Zhdankina, Y.S.; Sychev, V.N.; Orlov, O.I. Drosophila melanogaster Sperm under Simulated Microgravity and a Hypomagnetic Field: Motility and Cell Respiration. *Int. J. Mol. Sci.* **2020**, *21*, 5985. [CrossRef]

25. Islam, M.; Maffei, M.E.; Vigani, G. The Geomagnetic Field Is a Contributing Factor for an Efficient Iron Uptake in *Arabidopsis thaliana*. *Front. Plant Sci.* **2020**, *11*, 325. [CrossRef]

26. Maffei, M.E. Magnetic field effects on plant growth, development, and evolution. *Front. Plant Sci.* **2014**, *5*, 445. [CrossRef]

27. Maffei, M.E. Plant Responses to Electromagnetic Fields. In *Biological and Medical Aspects of Electromagnetic Fields*, 4th ed.; CRC Press: Boca Raton, FL, USA, 2018; pp. 89–110.

28. Fischer, J.; Laforsch, C. The influence of gravity and light on locomotion and orientation of *Heterocypris incongruens* and *Notodromas monacha* (Crustacea, Ostracoda). *NPJ Microgravity* **2018**, *4*, 3. [CrossRef]

29. Prasad, B.; Grimm, D.; Strauch, S.M.; Erzinger, G.S.; Corydon, T.J.; Lebert, M.; Magnusson, N.E.; Infanger, M.; Richter, P.; Krüger, M. Influence of Microgravity on Apoptosis in Cells, Tissues, and Other Systems In Vivo and In Vitro. *Int. J. Mol. Sci.* **2020**, *21*, 9373. [CrossRef]

30. Wehland, M.; Steinwerth, P.; Aleshcheva, G.; Sahana, J.; Hemmersbach, R.; Lützenberg, R.; Kopp, S.; Infanger, M.; Grimm, D. Tissue Engineering of Cartilage Using a Random Positioning Machine. *Int. J. Mol. Sci.* **2020**, *21*, 9596. [CrossRef]

31. Schüler, O.; Krause, L.; Görög, M.; Hauslage, J.; Kesseler, L.; Böhmer, M.; Hemmersbach, R. ARADISH—Development of a Standardized Plant Growth Chamber for Experiments in Gravitational Biology Using Ground Based Facilities. *Microgravity Sci. Technol.* **2016**, *28*, 297–305. [CrossRef]

32. Brungs, S.; Egli, M.; Wuest, S.L.; Christianen, P.C.M.; van Loon, J.J.W.A.; Anh, T.J.N.; Hemmersbach, R. Facilities for Simulation of Microgravity in the ESA Ground-Based Facility Programme. *Microgravity Sci. Technol.* **2016**, *28*, 191–203. [CrossRef]

33. Lyon, C.J. Choice of rotation rate for the horizontal clinostat. *Plant Physiol.* **1970**, *46*, 355–358. [CrossRef]

34. Muneer, S.; Kim, E.J.; Park, J.S.; Lee, J.H. Influence of Green, Red, and Blue Light Emitting Diodes on Multiprotein Complex Proteins and Photosynthetic Activity under Different Light Intensities in Lettuce Leaves (*Lactuca sativa* L.). *Int. J. Mol. Sci.* **2014**, *15*, 4657–4670. [CrossRef]

35. MongoDB. Available online: https://www.mongodb.com/ (accessed on 12 July 2024).

36. Rust. Available online: https://www.rust-lang.org/ (accessed on 12 July 2024).

37. Tokio—An asynchronous Rust Runtime. Available online: https://tokio.rs/ (accessed on 12 July 2024).

38. React. Available online: https://react.dev/ (accessed on 12 July 2024).

39. Electron. Available online: https://www.electronjs.org/ (accessed on 4 July 2024).

40. Mahavarkar, P.; John, J.; Dhapre, V.; Dongre, V.; Labde, S. Tri-axial square Helmholtz coil system at the Alibag Magnetic Observatory: Upgraded to a magnetic sensor calibration facility. *Geosci. Instrum. Method. Data Syst.* **2018**, *7*, 143–149. [CrossRef]

41. da Silva, R.C.; Ishioka, I.S.K.; Cappelletti, C.; Battistini, S.; Borges, R.A. Helmholtz Cage Design and Validation for Nanosatellites HWIL Testing. *IEEE Trans. Aerosp. Electron. Syst.* **2019**, *55*, 3050–3061. [CrossRef]
42. Goyal, T. Design and development of a three-axis controlled Helmholtz cage as an in-house magnetic field simulator for cubesats. In Proceedings of the International Astronautical Congress 2017, Adelaide, Australia, 25–29 September 2017.